NACA

RESEARCH MEMORANDUM

AVERAGE SKIN-FRICTION COEFFICIENTS FROM BOUNDARY-LAYER MEASUREMENTS IN FLIGHT ON A PARABOLIC BODY OF REVOLUTION (NACA RM-10) AT SUPERSONIC SPEEDS AND AT LARGE REYNOLDS NUMBERS

By Charles B. Rumsey and J. Dan Loposer

Langley Aeronautical Laboratory
Langley Field, Va.

NATIONAL ADVISORY COMMITTEE
FOR AERONAUTICS

WASHINGTON

March 7, 1951

NACA RM L51B12

NATIONAL ADVISORY COMMITTEE FOR AERONAUTICS

RESEARCH MEMORANDUM

AVERAGE SKIN-FRICTION COEFFICIENTS FROM BOUNDARY-LAYER MEASUREMENTS IN FLIGHT ON A PARABOLIC BODY OF REVOLUTION (NACA RM-10) AT SUPERSONIC SPEEDS AND AT LARGE REYNOLDS NUMBERS

By Charles B. Rumsey and J. Dan Loposer

SUMMARY

Boundary-layer measurements have been made on rocket-powered free-flight models to determine average skin-friction coefficients. The test body, designated NACA RM-10, was a fin-stabilized parabolic body of revolution of fineness ratio 12.2 with a blunt base to provide space for the rocket jet.

Average skin-friction coefficients were determined for two stations on the body. Three models were tested. Model 1 covered the Mach number range from 1.5 to 2.15, with a Reynolds number range from 89×10^6 to 139×10^6, based on body length to the measurement station; model 2 covered the Mach number range from 1.5 to 2.52, with a Reynolds number range from 57×10^6 to 124×10^6; and model 3 covered the Mach number range from 2.15 to 3.4, with a Reynolds number range from 42×10^6 to 160×10^6.

A significant decrease in skin-friction coefficient with increasing Mach number and Reynolds number is shown for both stations. Decreases in skin-friction coefficient of 10, 19, and 32 percent were measured over the ranges of models 1, 2, and 3, respectively. The magnitudes of the measured skin-friction coefficients are higher than those shown for a smooth flat plate at similar conditions by Van Driest's theory which considers heat transfer. However, the variations of the experimental skin-friction coefficients with Mach number and Reynolds number are quite similar to the variations shown by the theory.

INTRODUCTION

With the increased speeds of present and proposed aircraft and missiles, the need for experimental skin-friction data has increased. For low-drag missile configurations turbulent skin-friction drag at high speeds can account for as much as 50 percent of the total drag; hence, the accuracy of an estimate of total drag of such a missile configuration would depend to a large extent on the knowledge of skin-friction drag.

As the Mach number increases, the variations of the fluid properties within the boundary layer become significant due to effects of compressibility and aerodynamic heating. There have been several theories developed which predict a decrease in turbulent skin friction with an increase in Mach number, their difference being mainly in the assumptions of the variations of density, viscosity, and thermal conductivity within the boundary layer.

The earliest and most widely known theory was suggested by Von Kármán in 1935 (reference 1) and assumes that the fluid properties at the surface of the plate hold throughout the boundary layer. This gives the most extreme reduction in skin friction of any of the theories for a given increase in Mach number. More recent theories which consider a variation of fluid properties throughout the boundary layer have been given by Von Kármán and Tsien (reference 2), Frankl and Voishel, Kalikhman, Ferrari, Wilson, and Van Driest. These theories, with the exception of the first, are reviewed and compared with one of their own by Rubesin, Maydew, and Varga in reference 3. The theories differ widely in the amount of decrease in skin-friction coefficient predicted for a given increase in Mach number.

Only a meager amount of skin-friction data has been obtained at supersonic speeds. The measurements that have been made were at relatively low Reynolds numbers. Flat-plate skin-friction measurements at zero heat transfer from various sources were compared with the various theories for flat-plate turbulent flow in reference 3.

In order to obtain some needed skin-friction data on a body of revolution at high Mach numbers and Reynolds numbers, skin-friction measurements have been made by the National Advisory Committee for Aeronautics on a parabolic body of revolution of fineness ratio 12.2. The model, known as the NACA RM-10, was rocket-powered and fin-stabilized. The flight tests were made at the Pilotless Aircraft Research Station at Wallops Island, Va.

[redacted]

This paper presents average skin-friction coefficients as determined from boundary-layer total-pressure rake measurements using the boundary-layer momentum theorem. Rake measurements were made at stations 58 percent and 85 percent of the body length from the nose. The friction coefficients are average values for the body ahead of the measurement stations and were obtained over a Mach number range from 1.5 to 3.4 and over a Reynolds number range from 42×10^6 to 160×10^6 (based on axial body length to the measurement station).

SYMBOLS

M	Mach number
R_x	Reynolds number based on axial distance
R_θ	Reynolds number based on momentum thickness
C_f	average skin-friction coefficient
U	velocity, feet per second
u	velocity inside boundary layer, feet per second
T	temperature, $^\circ$F absolute
p	pressure, pounds per square foot
p_T	total pressure behind a normal shock wave
ρ	density, slugs per cubic foot
c_p	specific heat at constant pressure, 7.74 Btu per slug $^\circ$F for air
γ	ratio of specific heats, 1.4
J	mechanical equivalent of heat, 778 foot-pounds per Btu
g	acceleration due to gravity, 32.2 feet per second per second
k	thermal conductivity of air, Btu per foot-second $^\circ$F
μ	absolute viscosity, slugs per foot-second
σ	Prandtl number $\left(c_p\mu/k\right)$

[redacted]

x axial distance from nose of model, feet

s distance along surface from nose of model, feet

y distance normal from skin, feet

r radial distance from body axis, feet

A_x skin area back to station x, square feet

δ boundary-layer thickness, feet

δ^*_i incompressible boundary-layer displacement thickness, feet $\left(\int_0^\delta \left(1 - \frac{u}{U_\delta}\right)dy\right)$

δ^*_c compressible boundary-layer displacement thickness, feet $\left(\int_0^\delta \left(1 - \frac{u}{U_\delta}\frac{\rho}{\rho_\delta}\right)dy\right)$

θ_i incompressible boundary-layer momentum thickness, feet $\left(\int_0^\delta \frac{u}{U_\delta}\left(1 - \frac{u}{U_\delta}\right)dy\right)$

$H_i = \frac{\delta^*_i}{\theta_i}$

θ_c compressible boundary-layer momentum thickness, feet $\left(\int_0^\delta \frac{u}{U_\delta}\frac{\rho}{\rho_\delta}\left(1 - \frac{u}{U_\delta}\right)dy\right)$

β recovery factor $\left(\frac{T_{aw} - T_\delta}{T_s - T_\delta}\right)$

τ_w wall shearing stress, pounds per square foot

Subscripts:

1 free-stream conditions

w conditions at skin

[redacted]

δ	conditions just outside boundary layer
s	stagnation condition
av	average
aw	adiabatic wall condition

ANALYSIS

Average skin-friction drag coefficients were determined on the NACA RM-10 body by means of rake surveys of the total pressure through the boundary layer and static-pressure measurements at the rake location. The temperature through the boundary layer, which was needed for reduction of the pressure measurements, was determined from experimentally measured values of the skin temperature, known values of the temperature just outside the boundary layer, and a theoretical distribution of the temperature within the boundary layer, which is a function of the velocity distribution. The conditions of the flow within the boundary layer were then used in the momentum equation to obtain average skin-friction coefficients for the body ahead of the rake station. The integrated form of the boundary-layer equation for a body of revolution in steady flow can be obtained from reference 4 as

$$\frac{\partial}{\partial s}\int_0^{\delta} \rho u^2 r \, dy - U_\delta \frac{\partial}{\partial s}\int_0^{\delta} \rho u r \, dy = -\tau_w r_w + \rho_\delta U_\delta \frac{\partial U_\delta}{\partial s}\int_0^{\delta} r \, dy \qquad (1)$$

which can be written

$$\tau_w r_w = \frac{d}{ds}\int_0^{\delta} \left(\rho_\delta U_\delta^2 - \rho u^2\right) r \, dy - U_\delta \frac{d}{ds}\int_0^{\delta} \left(\rho_\delta U_\delta - \rho u\right) r \, dy \qquad (2)$$

For a slender body such as the RM-10, which has a basic-shape fineness ratio of 15, negligible error is caused by taking $dx = ds$ and $r = r_w + y$. Making these substitutions, integrating with respect to x, and using the definitions of δ^*_c and θ_c results in

[redacted]

$$\int_0^x \tau_w r_w \, dx = r_w \rho_\delta U_\delta^2 \theta_c + \int_0^x \rho_\delta U_\delta r_w \delta^*_c \frac{dU_\delta}{dx} \, dx +$$

$$\rho_\delta U_\delta^2 \int_0^\delta \left(\frac{\rho u}{\rho_\delta U_\delta} - \frac{\rho u^2}{\rho_\delta U_\delta^2} \right) y \, dy +$$

$$\int_0^x \frac{dU_\delta}{dx} \left[\rho_\delta U_\delta \int_0^\delta \left(1 - \frac{\rho u}{\rho_\delta U_\delta} \right) y \, dy \right] dx \tag{3}$$

The average friction coefficient for the part of the body ahead of the measurement station is then given by

$$C_f = \frac{\tau_{wav}}{q} = \frac{2\pi}{q A_x} \int_0^x \tau_w r_w \, dx \tag{4}$$

Evaluation of equation (3) requires a determination of the flow conditions through the boundary layer and of the conditions outside the boundary layer. Conditions outside the boundary layer were calculated from free-stream conditions using the body pressure distribution and the usual relations which assume isentropic flow behind the nose shock wave. The body pressure distribution was determined by using experimental static-pressure measurements and linear theory, which has been shown by wind-tunnel tests (reference 5) to predict closely the pressures over the RM-10 body.

With the static pressure assumed to be constant through the boundary layer, as is usual in boundary-layer theory, the Mach number variation through the boundary layer was determined from the total-pressure rake and static-pressure measurements using the supersonic pitot-tube equation

$$\frac{p_T}{p_\delta} = \frac{\left(\frac{\gamma + 1}{2} M^2 \right)^{\gamma/(\gamma-1)}}{\left(\frac{2\gamma}{\gamma + 1} M^2 - \frac{\gamma - 1}{\gamma + 1} \right)^{1/(\gamma-1)}} \tag{5}$$

[redacted]

The temperature distribution through the boundary layer was evaluated by using the theoretical relation given by Crocco in reference 6 which gives the temperature as a function of the velocity. This relation, which assumes a Prandtl number of 1 and steady-state conditions, was modified by the inclusion of the recovery factor β in order to obtain adiabatic wall temperature rather than stagnation temperature when the heat transfer is zero. The relation as used is

$$T = a + bu - \frac{\beta u^2}{2Jgc_p} \tag{6}$$

Evaluating the constants from the boundary conditions, $T = T_\delta$ at $u = U_\delta$ and $T = T_w$ at $u = 0$, and introducing the definition of adiabatic wall temperature

$$T_{aw} = T_\delta + \frac{\beta U_\delta^2}{2Jgc_p} \tag{7}$$

gives

$$T = T_\delta + \left(T_w - T_{aw}\right)\left(1 - \frac{u}{U_\delta}\right) + \frac{\beta\left(U_\delta^2 - u^2\right)}{2Jgc_p} \tag{8}$$

The second term on the right-hand side of equation (8) represents the effect of heat transfer and is equal to zero when the skin temperature is equal to the adiabatic wall temperature. For the present tests, values of T_w, T_{aw}, and β were determined from experimental measurements made on RM-10 models in the supersonic convective heat-transfer phase of the RM-10 program (reference 7).

By means of equation (8) the measured Mach number distribution was converted to velocity and temperature distribution. The density distribution was obtained from the relation $\frac{\rho}{\rho_\delta} = \frac{T_\delta}{T}$.

In order to evaluate the first integral on the right-hand side of equation (3), the variation of δ^*_c with x was assumed to be linear from a value of zero at the nose to the value determined at the measurement station. This approximation is believed to be satisfactory since the magnitude of the term in which δ^*_c appears is only approximately 5 percent of the other terms of equation (3). The last term of equation (3) was neglected since it is many times smaller than the term containing δ^*_c which, as stated above, is small.

[redacted]

The integrals in equation (3) were evaluated graphically and the final results when used in equation (4) gave the average skin-friction coefficients for the body ahead of the rake measurement station.

MODELS AND TESTS

Three models were flown for the tests reported herein. Model 3 was a standard NACA RM-10 test vehicle as were models 1 and 2, except for modification to their tail sections. The general configuration and body equation of the RM-10 test vehicle are shown in figure 1. The body is of parabolic-arc profile, the basic parabolic shape having a fineness ratio of 15. Cutting off the pointed stern at 81.25 percent of the full length to allow space for the rocket jet results in an actual body fineness ratio of 12.2. Four untapered stabilizing fins with leading edges swept back 60° are equally spaced around the stern. The total aspect ratio is 2.04. The cross section of the fins normal to the leading edge is circular arc with a fineness ratio of 10 percent. This results in a fineness ratio of 5 percent in the streamwise direction. The fins are constructed of cast magnesium and are attached to a cast-magnesium tail section, whereas the body skin is spun from magnesium sheet.

All models were made as nearly identical as possible ahead of station 128. However, in order to simplify the construction of models 1 and 2, the standard RM-10 tail section starting at station 128 was replaced on these two models with a cylindrical tail section carrying wooden fins. The fins of these two models had a delta plan form with leading edges swept back 45°.

Unpublished test data from the Langley 4- by 4-foot supersonic tunnel on the RM-10 configuration at a Mach number of 1.4 and a Reynolds number of 3.6×10^6, and with an artificially caused turbulent boundary layer, show no variation in body-static-pressure distribution ahead of the fin location due to addition of the fins. Since the leading edges of the wooden fins were wedge-shaped, with a smaller included angle than that of the standard RM-10 fins, it is assumed that the change in fin design had no effect on the pressures at the measurement station.

The RM-10 body was designed with only one lightweight bulkhead and three lightweight joints in order to keep to a minimum the distortion of the body shape caused by the restraint of bulkheads as the skin temperature changes under the influence of aerodynamic heating.

The Deacon rocket motor (JATO 3.5-ES-5700, X204A1) was selected as the internal rocket because of the low temperature of its case during burning. Since the case reaches only approximately 150° F during burning, it has negligible effect on the skin temperature of the model.

[redacted]

Profile measurements of body contours were made on all models. The agreement between the radii, as given by the equation of the body and the measured radii, was within 0.02 inch.

The models were highly polished immediately prior to launching. Measurements of skin roughness were made using a Brush surface analyzer with a stylus tip radius of 0.0005 inch. The measurements indicated a maximum surface roughness of 50 microinches with an average value of approximately 25 microinches. This degree of smoothness is roughly comparable to that of a polished fine-ground surface.

The 6.25-inch ABL Deacon rocket motors used to propel the models had a total impulse of approximately 19,800 pound-seconds. Model 3 was boosted by a second 6.25-inch ABL Deacon motor which was drag-separated from the model at cessation of its thrust. Figure 2 is a photograph of this model in launching position.

The distribution of total pressure through the boundary layer was measured at station 125 on models 1 and 3 and at station 85 on model 2 by means of a six-tube total-pressure rake. The rake configurations used at stations 85 and 125 are shown in figure 3. The total-pressure tubes were mounted in a rake blank having a chordwise thickness ratio of 10.7 percent and sharp leading and trailing edges of 21° wedge angle. The tubes were made of stainless steel and each had a 0.09-inch outside diameter and a 0.06-inch inside diameter with the mouth pinched down to a 0.04-inch opening and the wall honed to a maximum of 0.01-inch thickness at the lip.

Body static pressure was measured at the measurement station 180° around the body from the rake installation by a $\frac{1}{8}$-inch-diameter flush orifice in the skin.

Pressures and longitudinal acceleration were measured on the body by standard NACA instrumentation and the data telemetered during flight to two ground receiving stations. Atmospheric data were obtained from radiosonde observations made at the time of the tests. Velocity and position of the model along the flight trajectory were measured by Doppler velocity radar and a radar tracking unit. In the case of the boosted model 3, which exceeded the range of the Doppler velocimeter, velocity data were obtained by integrating the record of longitudinal acceleration.

The unboosted models 1 and 2 were launched at an elevation of approximately 55°. Maximum Mach number was reached near burnout of the rocket motor, which was approximately 3.2 seconds after launching. The model then coasted upward with decreasing velocity, during which time the test data were obtained. The boosted model, number 3, was launched at an angle of elevation of approximately 70°. The booster rocket burned

[redacted]

out and separated approximately 3.2 seconds after launching. A delay of approximately 9 seconds after booster separation was allowed before firing of the internal sustainer rocket. The sustainer rocket fired for approximately 3.2 seconds, after which the test data were obtained during the upward coasting period of flight. Figure 4 shows the variation of Mach number with time for each of the three models and indicates the intervals over which the data were obtained.

Figure 5 shows the Reynolds number, based on body length to the measurement station, plotted against Mach number for each of the three models. Also shown is Reynolds number based on the experimentally determined momentum thickness θ_c.

RESULTS AND DISCUSSION

In order to evaluate skin-friction and boundary-layer velocity profiles, it is necessary to determine the Mach number and temperature distributions through the boundary layer. The Mach number distribution through the boundary layer at the measurement station was found directly from the measurements of the rake total-pressure tubes and the body static-pressure orifice. The temperature of the skin T_w, which varied considerably during the flight, was determined from experimental measurements on RM-10 bodies (as reported in reference 7). The ratio of skin temperature to temperature just outside the boundary layer T_w/T_δ is plotted against Mach number in figure 6 for the test range of each model to show the variation of the skin temperature and also for use later in considering the effect of heat transfer on C_f. There was a temperature gradient along the body which varied during the flight from -1° F per inch to 0.5° F per inch for model 3 and from -0.5° F per inch to approximately 0 for models 1 and 2. Primarily because of this, the ratio T_w/T_δ is not constant along the body at a given time. Figure 6, therefore, shows the value of the ratio occurring at the "average-area station" ahead of the measurement station as being indicative of the conditions of heating of the body ahead of the measurement station.

Typical temperature distributions through the boundary layer at the rake station of model 3, determined from equation (8), are shown in figure 7 for several times after launching. They are presented as a plot of temperature referred to the temperature outside the boundary layer against velocity referred to the velocity outside the boundary layer.

At 15.14 and 17.10 seconds the skin is being strongly heated, as can be judged by the positive temperature gradients in the boundary layer. At 21.15 seconds the temperature gradient at the skin is zero, the skin being in thermal equilibrium with the boundary layer. At

[redacted]

25.00 seconds the temperature gradient is negative and the skin is being cooled.

By use of the corresponding temperature distributions, the curves of Mach number through the boundary layer were converted to velocity. The velocity distributions for the maximum and minimum test Mach numbers of each of the three models are shown in figure 8 with velocity u plotted against distance from the skin y. The measured boundary-layer velocity distributions for the two measurement stations are shown in figure 9 as nondimensional plots of velocity referred to the velocity outside the boundary layer plotted against distance out from the skin referred to θ_i.

The incompressible momentum thickness θ_i was used to reduce y to nondimensional form because its value is easily and accurately determined directly from the velocity profiles. Values of the incompressible boundary-layer parameter H_i defined as δ^*_i/θ_i, can be obtained directly for each condition by integrating the nondimensional velocity profile curves of figure 9. Although it cannot be shown analytically that the velocity profile is a function only of H_i, it has been shown experimentally in reference 8 that all the turbulent velocity profiles measured in incompressible flow are approximately functions of the single parameter H_i. In reference 9 it has been shown that the nondimensional velocity profile shape of a turbulent boundary layer is approximately a function of the single parameter H_i for compressible flow to a Mach number of 1.2, as well as for incompressible flow. Reference 9 also shows that the functional relation between H_i and the profile shape is the same for compressible flow as for incompressible flow.

In order to determine if the same functional relation between the velocity profile and H_i holds above Mach numbers of 1.2, the data of the present tests have been plotted in figure 10 in the form of u/U_δ against H_i for various values of y/θ_i. The solid lines represent the faired data of reference 8 and the broken lines represent the faired data of reference 9, while the data points are from the present tests. Since all the data points define, without excessive scatter, a single curve of u/U_δ against H_i for each value of y/θ_i, it may be concluded that the nondimensional velocity profile shapes are approximately a function of the single parameter H_i over the range of these tests. The agreement between the data from the present high Mach number tests and the curves representing the data from references 8 and 9 also indicates that the functional relation between H_i and the profile shape is unchanged by Mach number.

[redacted]

Evaluating equation (4), using the body area ahead of the measurement station, gives average skin-friction coefficients for the body surface ahead of the measurement station. Except possibly at the low Reynolds numbers attained at high altitude on model 3, these experimental values can be considered average friction coefficients for turbulent flow. This is because of the predominance of turbulent boundary layer, in respect to area, back to the measurement stations. Results of a flight measurement of transition on the RM-10 nose section, which are as yet unpublished, indicated that transition occurred at station 10 at a Reynolds number of approximately 8×10^6, based on body length to the station. If this value of Reynolds number for transition at station 10 is applicable at other stations, it would place transition within the first 12 inches of body length for the complete test ranges of models 1 and 2 and for the upper half of the Mach number range of model 3. With transition occurring ahead of station 12, more than 97.4 percent of the skin area ahead of either measurement station has turbulent boundary layer. Thus, there is little error in considering the average coefficients in these conditions as those for turbulent flow.

There is no compressible turbulent boundary-layer theory available which predicts the magnitude of the skin friction or its variation with Mach number, Reynolds number, and heat transfer for a body of revolution. However, the variation of C_f with these parameters for a slender body of revolution should be similar to that for a flat plate if r is large with respect to δ.

An analysis for the average turbulent friction on a smooth flat plate, which includes heat transfer, has recently been made by Van Driest (reference 10). His assumptions include a constant skin temperature along the plate and the usual boundary-layer assumptions, Prandtl number of 1, and steady-state conditions. His equation relates C_f, Mach number, Reynolds number, and the ratio of wall temperature to temperature outside the boundary layer T_w/T_δ. Theoretical values of C_f for a flat plate were computed for the range of conditions covered by each test model. The values of the ratio T_w/T_δ used were those occurring at the average-area station ahead of the rake station (as given in fig. 6).

The experimental values of C_f and the corresponding theoretical curves of flat-plate C_f are plotted against Mach number in figure 11. The Reynolds numbers occurring at the extremities of the test ranges are shown on the experimental curves. Although the experimental values are considerably higher, the variations of the experimental curves and of the theoretical flat-plate curves are similar. Both the experimental curve and the theoretical flat-plate curve show a reduction in C_f of approximately 10 percent over the range of model 1. Both show a reduction of approximately 19 percent over the range of model 2. The

[redacted]

experimental curve for model 3, which reaches the high Mach number of 3.4, shows a reduction in C_f of about 32 percent, while the theoretical flat-plate curve shows a reduction of approximately 25 percent.

The experimental values of C_f for the body of revolution are from 12 to 33 percent higher than the corresponding theoretical values for a flat plate. This might be expected because of the three-dimensional character of the body, as pointed out in reference 11 for the case of laminar flow. Part of this discrepancy may also be due to limitations in the flat-plate theory itself.

It is apparent in figure 11 that models 1 and 3 have the same C_f at the common Mach number of 2.15, although the Reynolds number of model 1 is 139×10^6 and that of model 3 is 42×10^6. If the higher Reynolds number of model 1 was the only difference in conditions, its C_f would be expected to be lower than that of model 3. Actually, however, although the heat transfer on model 3 is negligible at this Mach number, model 1 still has a cool skin since it just attained peak velocity and is therefore cooling the boundary layer, thus raising the C_f and masking the expected Reynolds number effect.

The values of C_f measured at station 85 on model 2 should not be compared in magnitude with values of C_f measured at station 125 on models 1 and 3, since the over-all effects of the body shape and pressure distribution on the boundary layer were different for the two stations. It is interesting to note that the values of C_f measured on model 2 at station 85 are lower than those measured on model 1 at station 125, although the reverse might be expected in view of the pressure gradients on the forward part of the body. There is no apparent explanation for this occurrence. However, the decrease in C_f measured at station 85 over the range of model 2 is similar to that measured at station 125 and, as already mentioned, is in good agreement with the decrease shown by its corresponding theoretical flat-plate curve.

The experimental and theoretical curves of figure 11 are replotted in figure 12 as a logarithmic plot of C_f against Reynolds number. On this plot the variations of Reynolds number through the test ranges are apparent. The Reynolds number increase which accompanies the increase in Mach number over each test range doubtless causes part of the reduction in C_f measured on each model, but its effect cannot be separated from the effects of Mach number and heat transfer, since the separate effect of none of these variables can be determined from the limited data of the present tests.

For each of the theoretical flat-plate C_f curves, however, the effect of each variable can be separately determined. Figure 13 shows

[redacted]

the theoretical flat-plate C_f curves as in figure 11, along with a corresponding curve for each range computed from Van Driest's equation, with the skin temperature being that of an insulated flat plate - that is, no heat transfer. The large heat flow into the skin, which occurs at the highest Mach number for each model, causes a large increase in the theoretical flat-plate C_f due to the lowering of the temperature (that is, increasing density) of the boundary layer. At the lowest Mach numbers, the conditions of heat transfer on each model were different. Model 1 was still being heated at its lowest Mach number, with the accompanying increase in theoretical flat-plate C_f. Model 2 was being heated only slightly, with a consequent small increase in flat-plate C_f. Model 3 was being cooled slightly, which caused a small decrease in the theoretical flat-plate C_f.

The theoretical curve which covers the Mach and Reynolds number range of model 3, but assumes no heat transfer, shows a decrease in C_f of approximately 42 percent, with the Reynolds number change causing a 21-percent decrease and the Mach number change also causing a 21-percent decrease. The theoretical curve for model 3 with heat transfer has a decrease in C_f of approximately 25 percent, as mentioned before in reference to figure 11. The decrease in C_f caused by the change in Reynolds number is still 21 percent, with a decrease of 5 percent being caused by the change in Mach number. It can be seen that the theoretically predicted change in C_f due to a variation of Reynolds number is relatively unaffected by the presence or absence of heat transfer. The theoretically predicted change in C_f due to variation in Mach number is, however, very dependent on the variation of heat-transfer conditions, and the theory indicates that greater reductions in C_f than those measured would probably be present with no heat transfer.

CONCLUDING REMARKS

Average skin-friction coefficients have been determined experimentally for two stations on a parabolic body of revolution of fineness ratio 12.2 (NACA RM-10) by measuring the momentum loss in the boundary layer. Three rocket-powered models were used in the tests. Model 1 covered the Mach number range from 1.5 to 2.15, with a Reynolds number range from 89×10^6 to 139×10^6, based on body length to the measurement station; model 2 covered the Mach number range from 1.5 to 2.52, with a Reynolds number range from 57×10^6 to 124×10^6; and model 3 covered the Mach number range from 2.15 to 3.4, with a Reynolds number range from 42×10^6 to 160×10^6.

The experimental measurements show a significant decrease in skin-friction coefficient with increasing Mach number and Reynolds number over

[redacted]

the range of the tests. Decreases in skin-friction coefficient of 10, 19, and 32 percent were measured over the ranges of models 1, 2, and 3, respectively. The magnitudes of the measured skin-friction coefficients are higher than those shown for a smooth flat plate at similar conditions by Van Driest's theory which considers heat transfer. However, the variations of the experimental skin-friction coefficients with Mach number and Reynolds number are quite similar to the variations shown by the theory.

The test measurements show that the boundary-layer velocity profile shape is a function of the single parameter H_1 for compressible flow over the entire test Mach number range, as well as for incompressible flow.

Langley Aeronautical Laboratory
National Advisory Committee for Aeronautics
Langley Field, Va.

[redacted]

REFERENCES

1. Von Kármán, Th.: The Problem of Resistance in Compressible Fluids. R. Accad. d'Italia, vol. XIV, 1936. (Fifth Volta Congress held in Rome, Sept. 30 - Oct. 6, 1935.)

2. Von Kármán, Th., and Tsien, H. S.: Boundary Layer in Compressible Fluids. Jour. Aero. Sci., vol. 5, no. 6, April 1938, pp. 227-232.

3. Rubesin, Morris W., Maydew, Randall C., and Varga, Steven A.: An Analytical and Experimental Investigation of the Skin Friction of the Turbulent Boundary Layer on a Flat Plate at Supersonic Speeds. NACA TN 2305, 1951.

4. Fluid Motion Panel of the Aeronautical Research Committee and Others: Modern Developments in Fluid Dynamics. Vol. I, S. Goldstein, ed., The Clarendon Press (Oxford), 1938, p. 133.

5. Luidens, Roger W., and Simon, Paul C.: Aerodynamic Characteristics of NACA RM-10 Missile in 8- by 6-Foot Supersonic Wind Tunnel at Mach Numbers from 1.49 to 1.98. I - Presentation and Analysis of Pressure Measurements (Stabilizing Fins Removed). NACA RM E50D10, 1950.

6. Crocco, Luigi: Transmission of Heat from a Flat Plate to a Fluid Flowing at a High Velocity. NACA TM 690, 1932.

7. Chauvin, Leo T., and deMoraes, Carlos A.: Correlation of Supersonic Convective Heat-Transfer Coefficients from Measurements of the Skin Temperature of a Parabolic Body of Revolution (NACA RM-10). NACA RM L51A18, 1951.

8. Von Doenhoff, Albert E., and Tetervin, Neal: Determination of General Relations for the Behavior of Turbulent Boundary Layers. NACA Rep. 772, 1943.

9. Tulin, Marshall P., and Wright, Ray H.: Investigation of Some Turbulent-Boundary-Layer Velocity Profiles at a Tunnel Wall with Mach Numbers up to 1.2. NACA RM L9H29a, 1949.

10. Van Driest, E. R.: The Turbulent Boundary Layer for Compressible Fluids on a Flat Plate with Heat Transfer. Rep. No. AL-997, North American Aviation, Inc., Jan. 27, 1950.

11. Mangler, W.: Compressible Boundary Layers on Bodies of Revolution. Reps. and Translations No. 47, British M.A.P. Völkenrode, March 15, 1946.

[redacted]

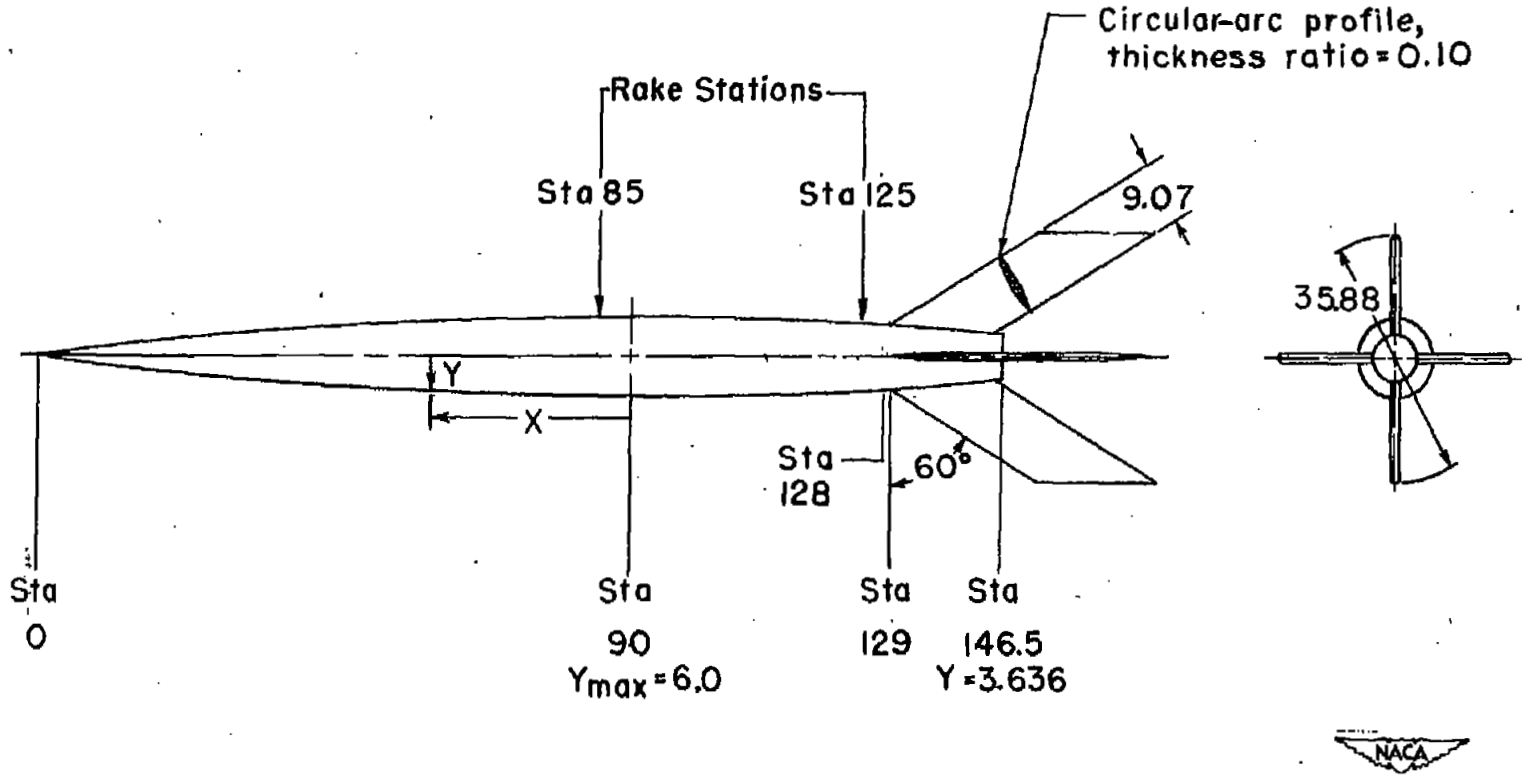

Body profile equation

$$Y = 6.000 - .0007407\,X^2$$

Figure 1.- General configuration and body equation of the NACA RM-10. Dimensions are in inches.

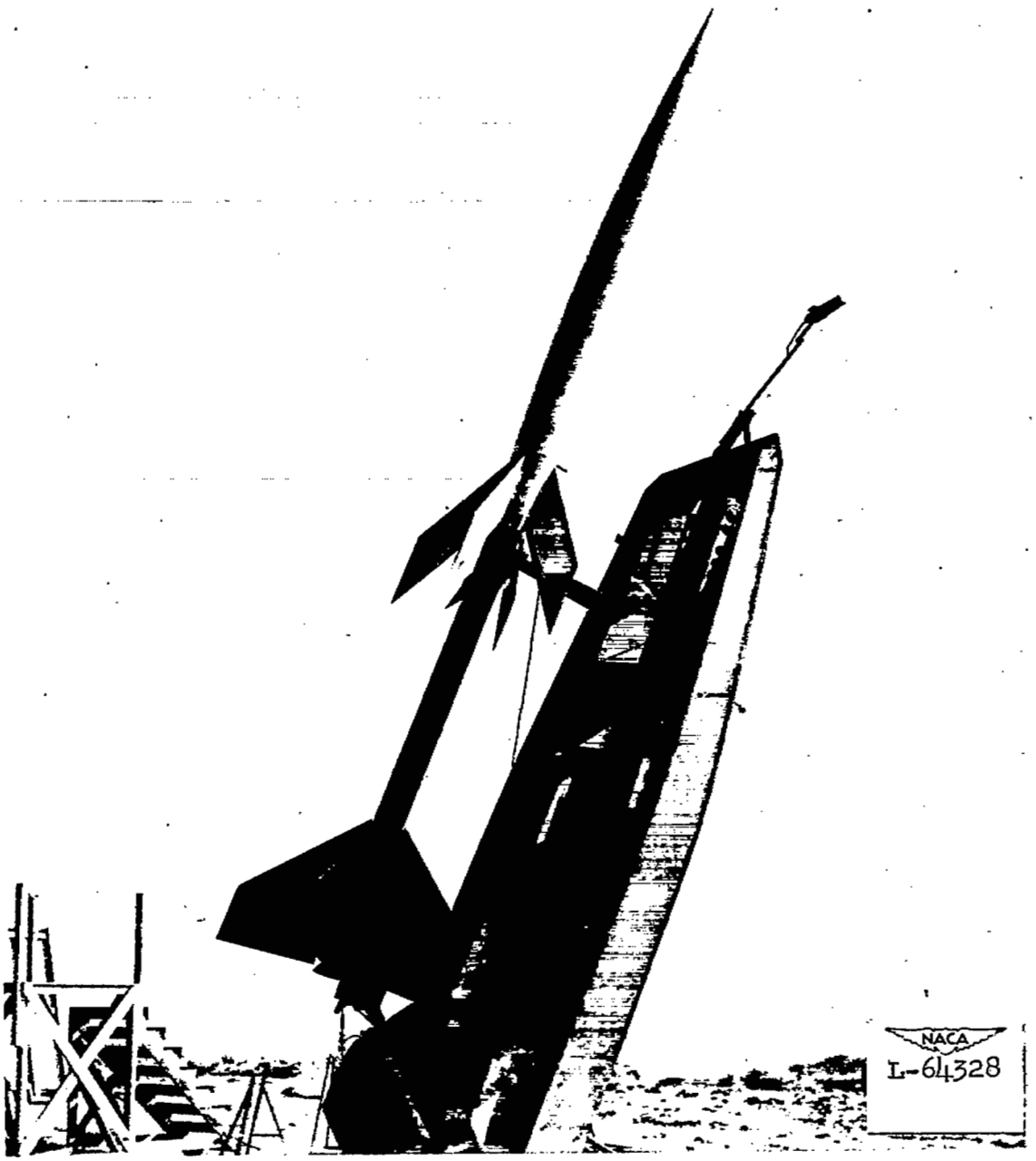

Figure 2.- Model 3 in launching position.

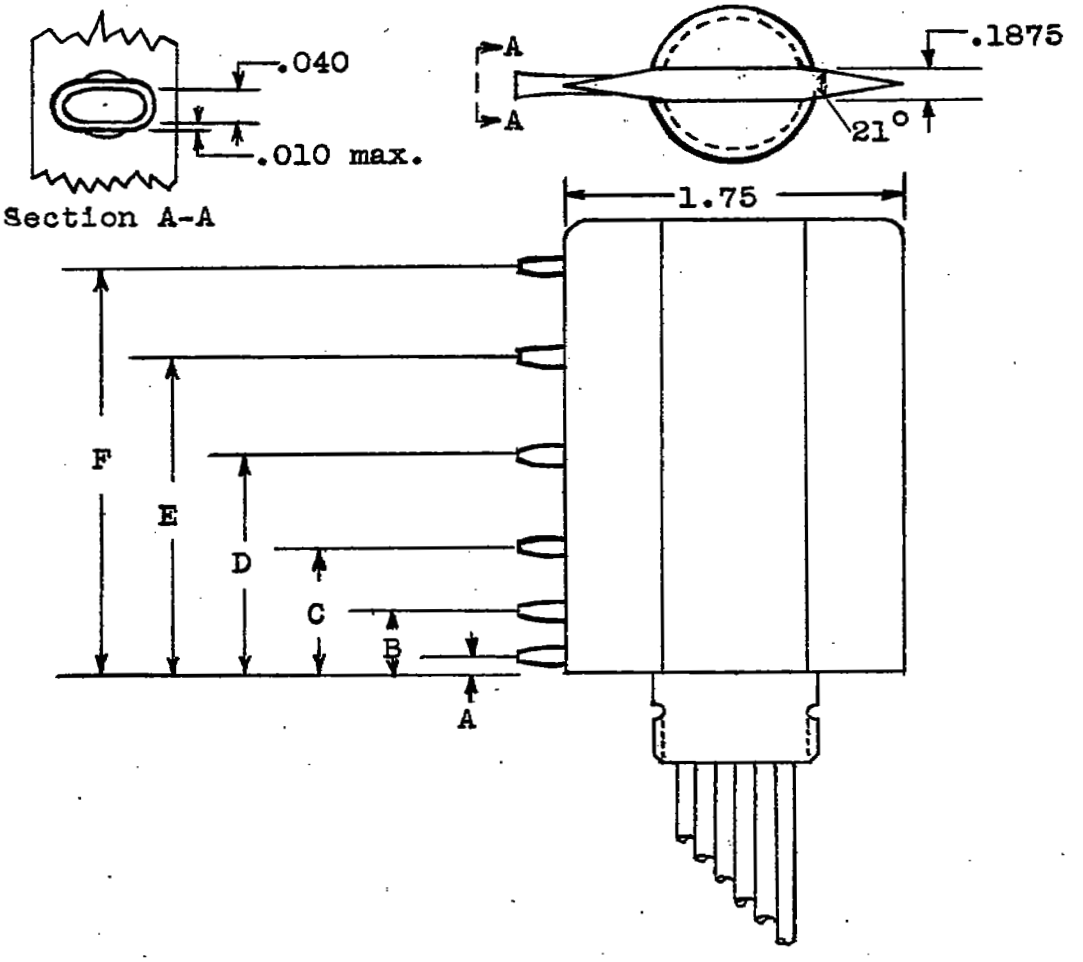

Tube	Model 1	Model 2	Model 3
A	0.08	0.06	0.05
B	.29	.20	.35
C	.65	.35	.65
D	1.41	.58	1.15
E	1.65	1.00	1.75
F		1.50	2.50

Figure 3.- General configuration of total-pressure rakes and spacing of tubes. Dimensions are in inches.

[redacted]

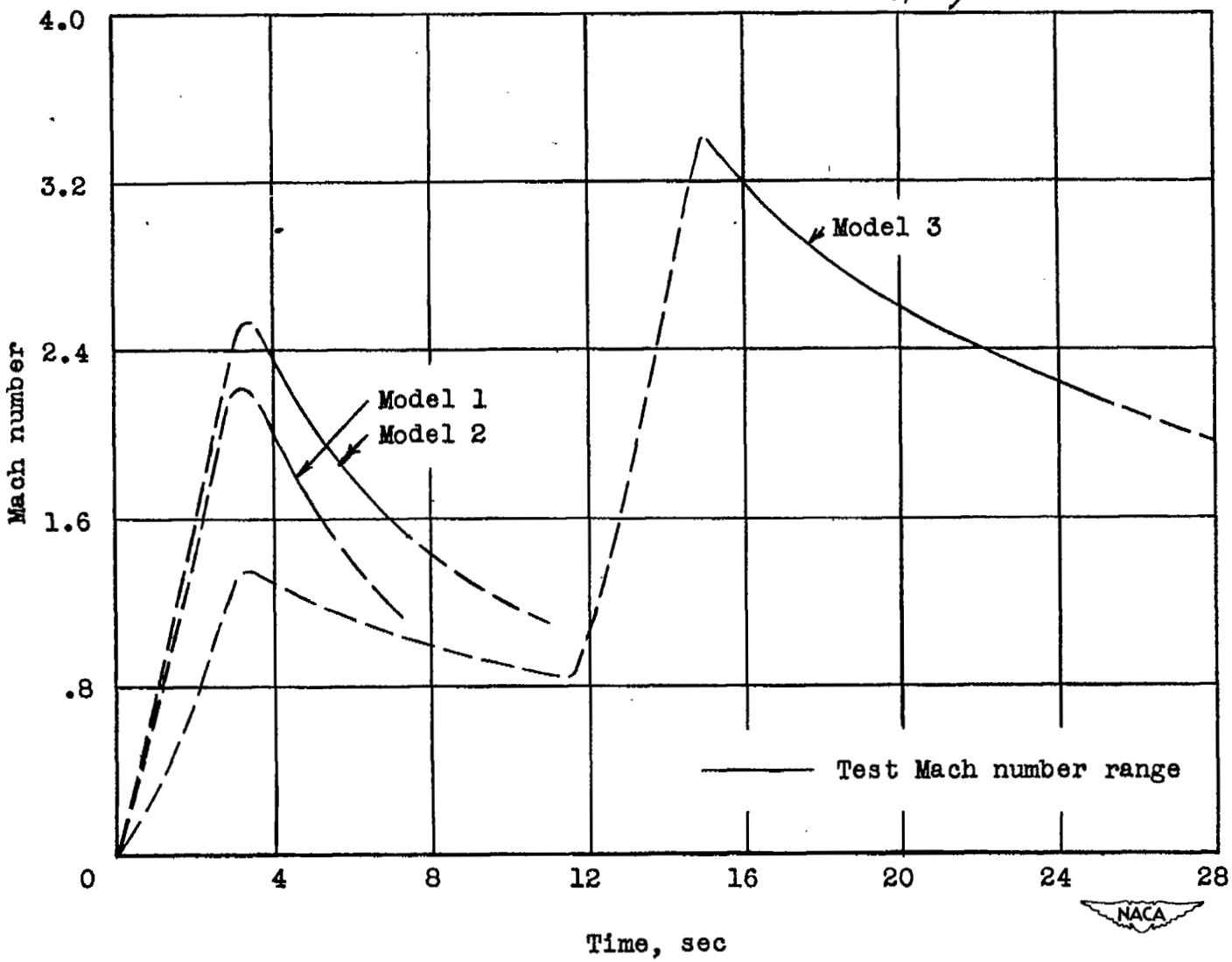

Figure 4.- Mach number against time for test models.

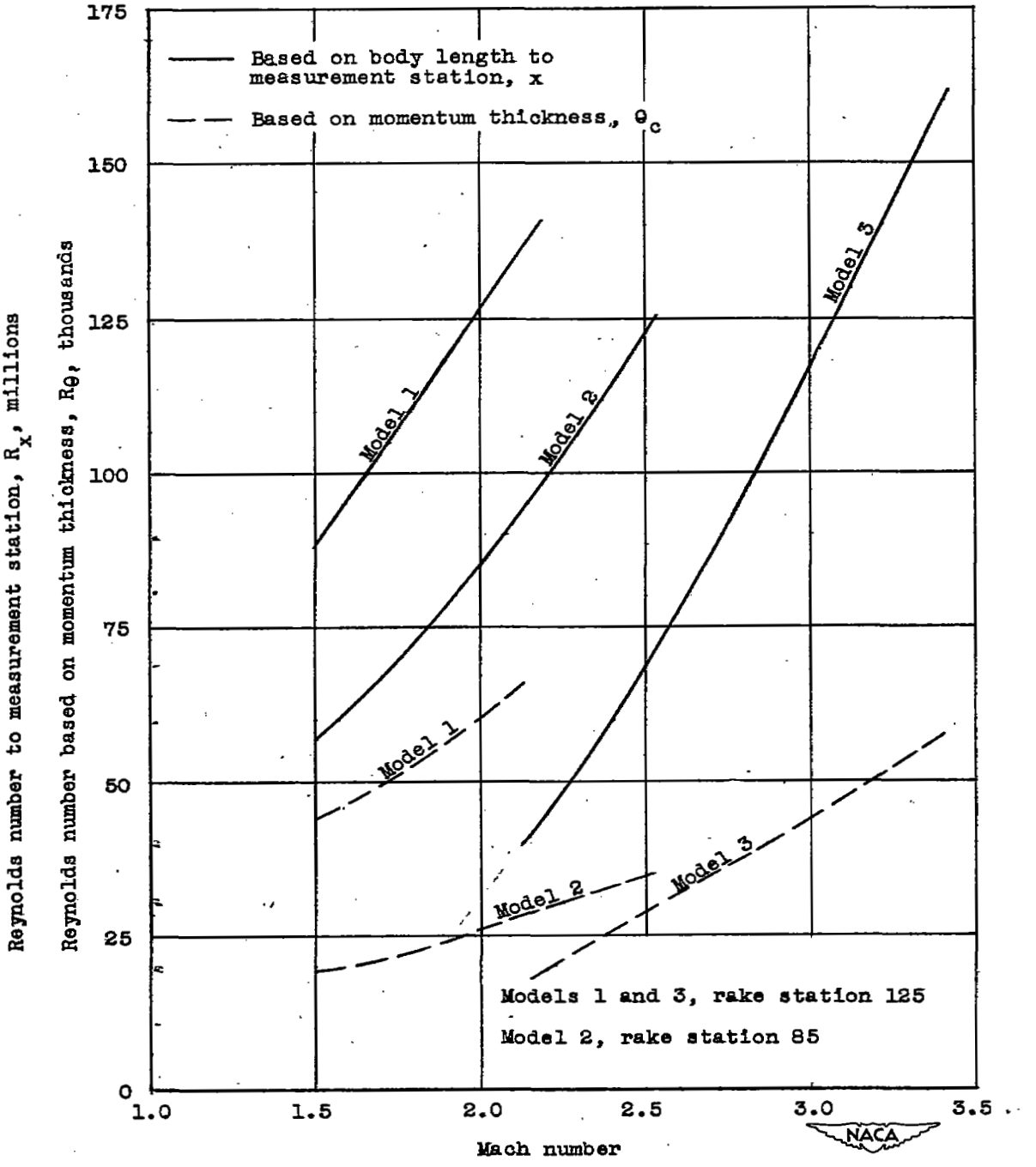

Figure 5.- Variation of Reynolds number with Mach number for the test models.

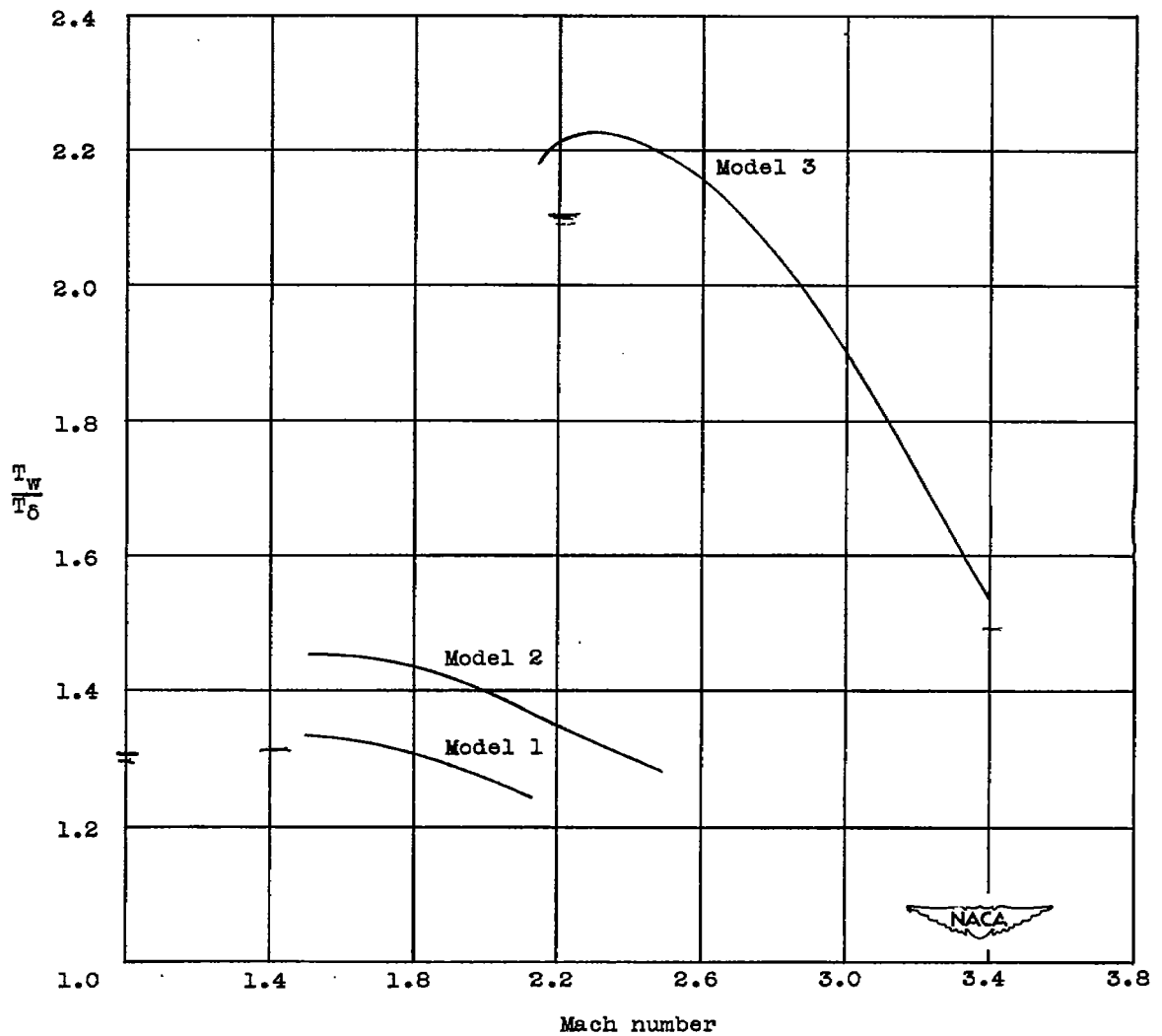

Figure 6.- Variation of heat-transfer parameter $\frac{T_w}{T_\delta}$ with Mach number.

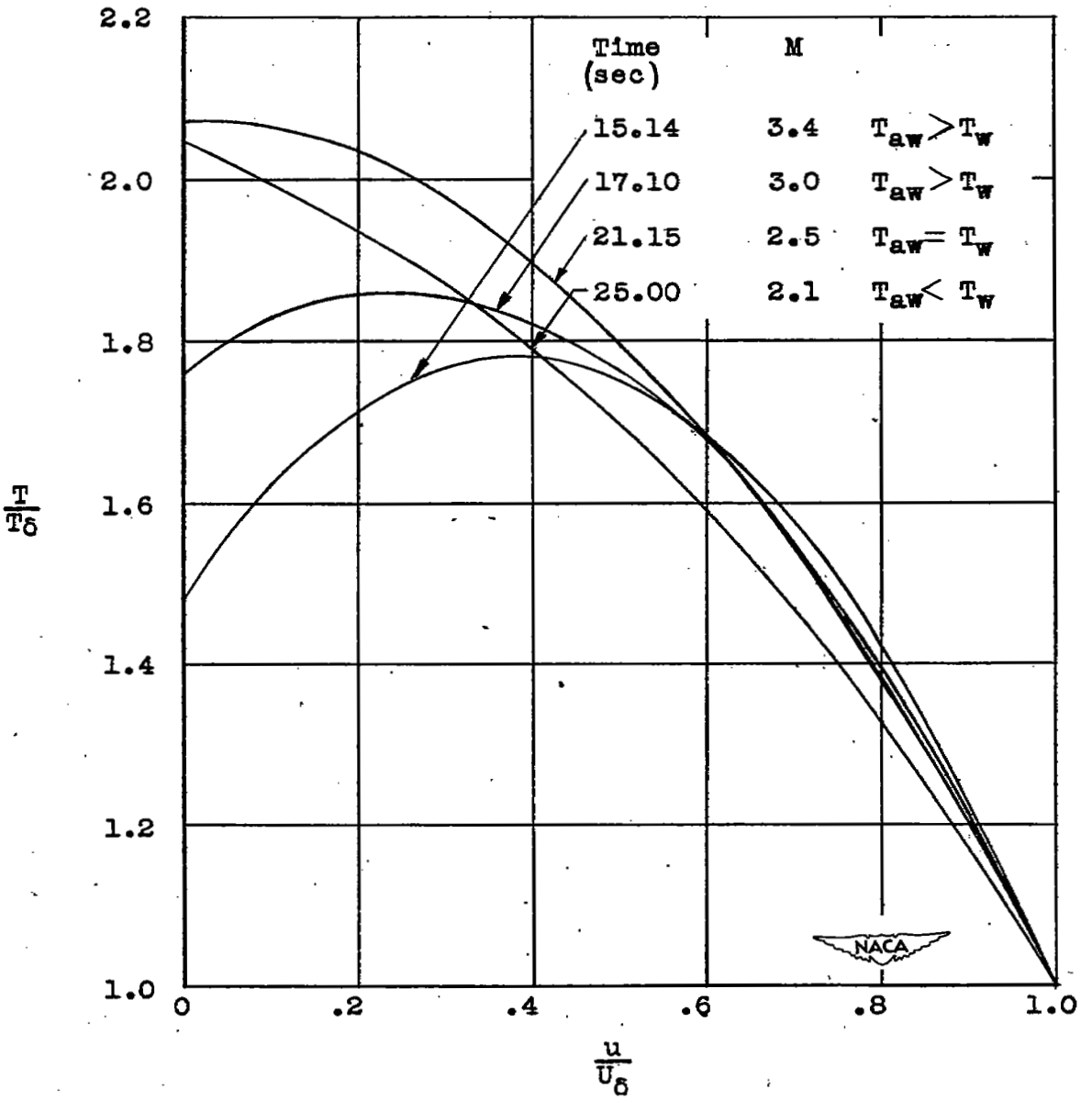

Figure 7.- Typical nondimensional boundary-layer temperature distributions.

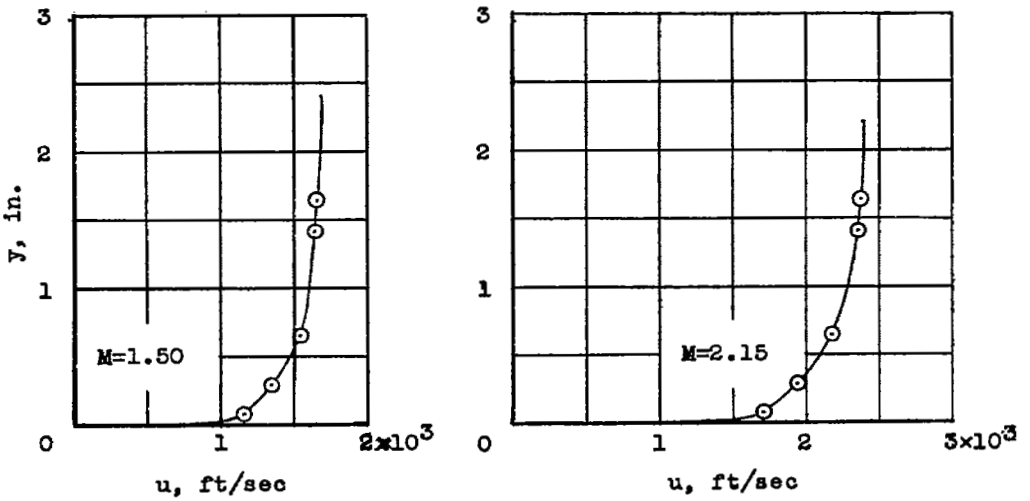

(a) Model 1; station 125.

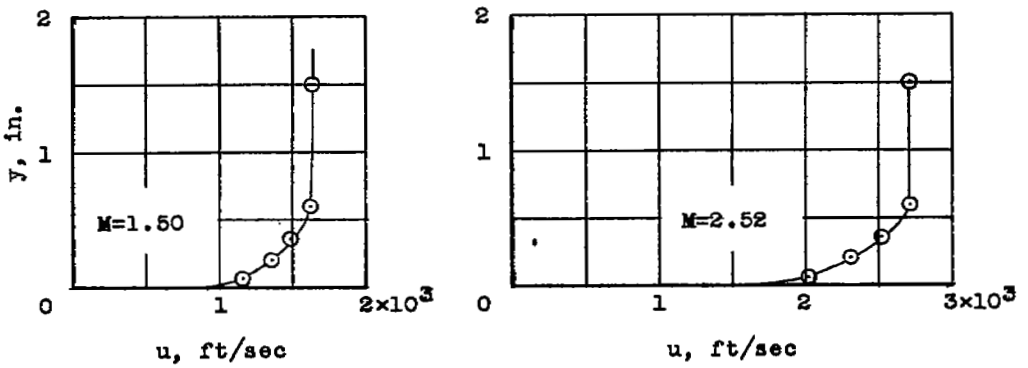

(b) Model 2; station 85.

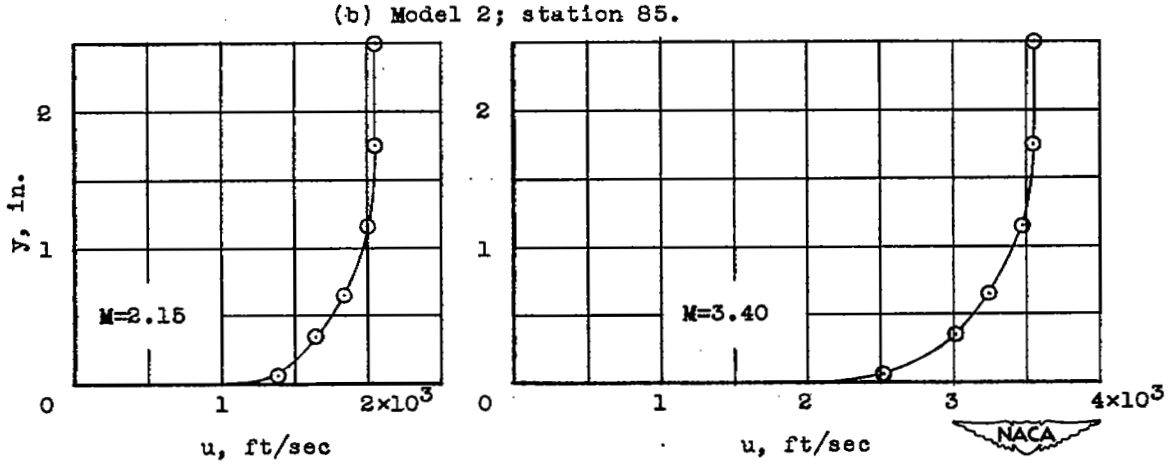

(c) Model 3; station 125.

Figure 8.- Velocity distributions at the maximum and minimum test Mach numbers for each model.

[redacted]

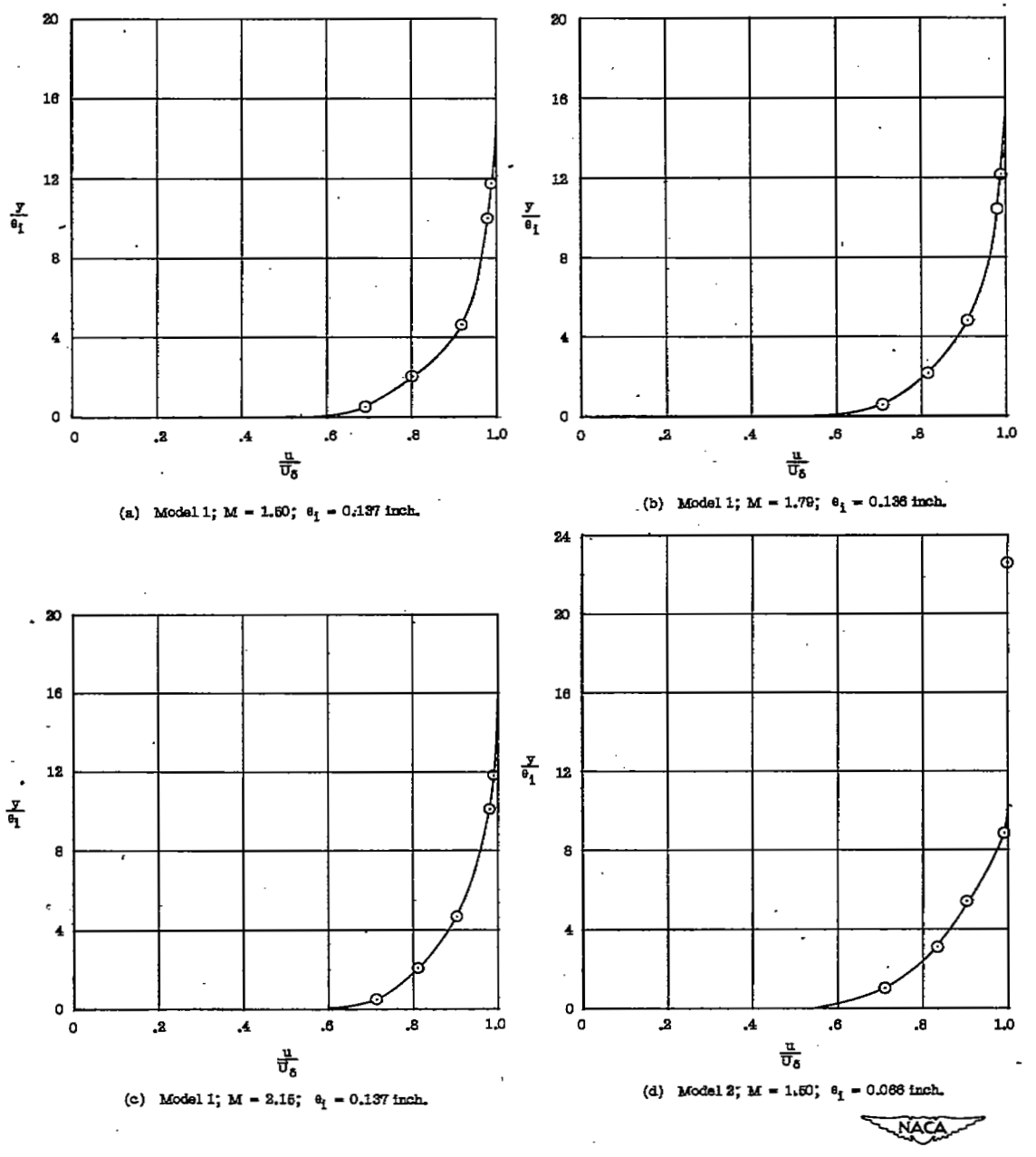

(a) Model 1; M = 1.60; θ_i = 0.137 inch.

(b) Model 1; M = 1.79; θ_i = 0.136 inch.

(c) Model 1; M = 2.15; θ_i = 0.137 inch.

(d) Model 2; M = 1.60; θ_i = 0.066 inch.

Figure 9.- Nondimensional boundary-layer velocity profiles.

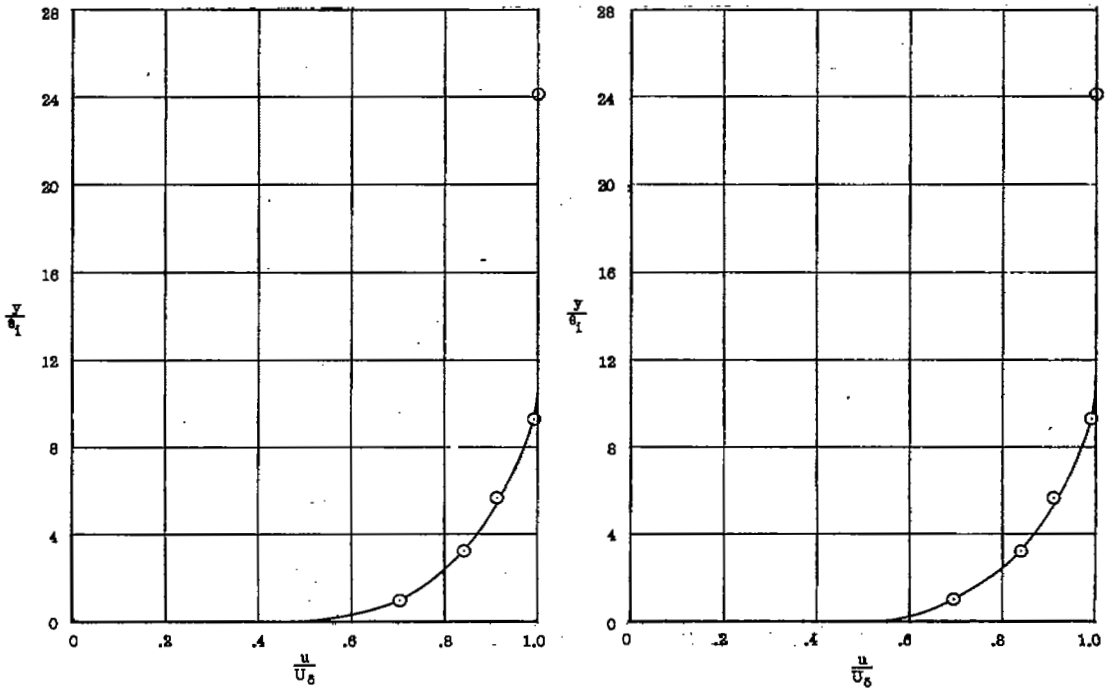

(e) Model 2; M = 1.75; θ_i = 0.062 inch.

(f) Model 2; M = 2.00; θ_i = 0.062 inch.

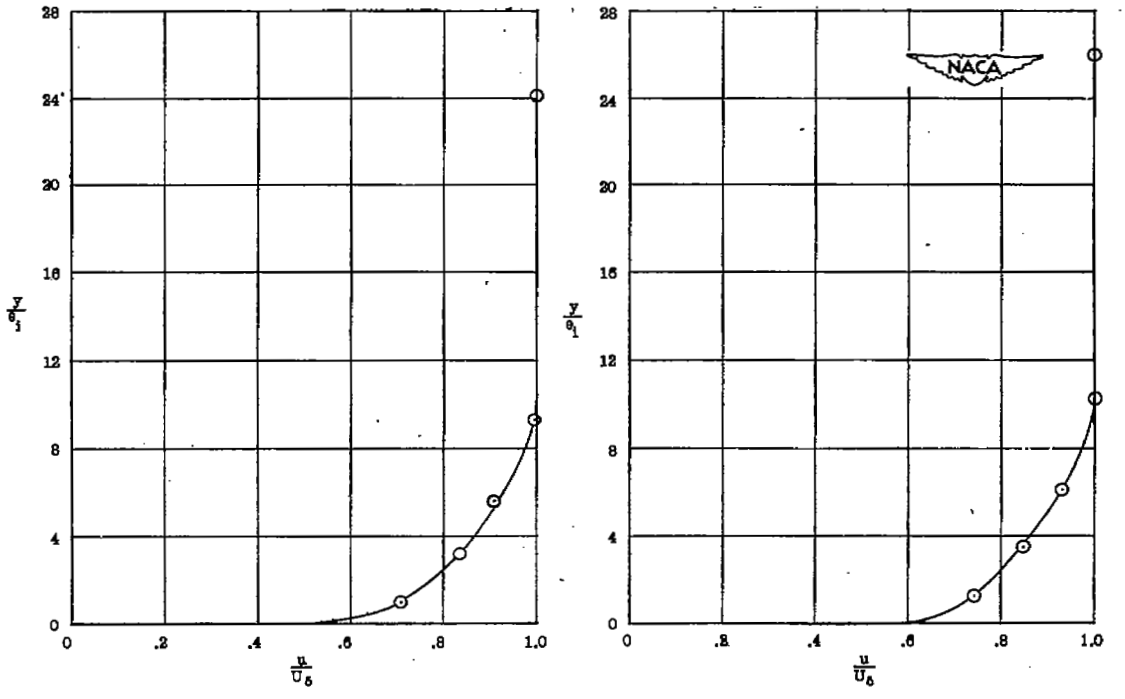

(g) Model 2; M = 2.25; θ_i = 0.062 inch.

(h) Model 2; M = 2.52; θ_i = 0.058 inch.

Figure 9.- Continued.

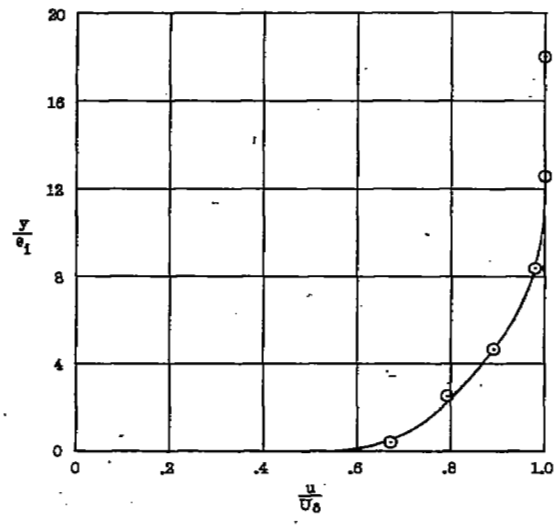

(i) Model 3; M = 2.15; θ_1 = 0.139 inch.

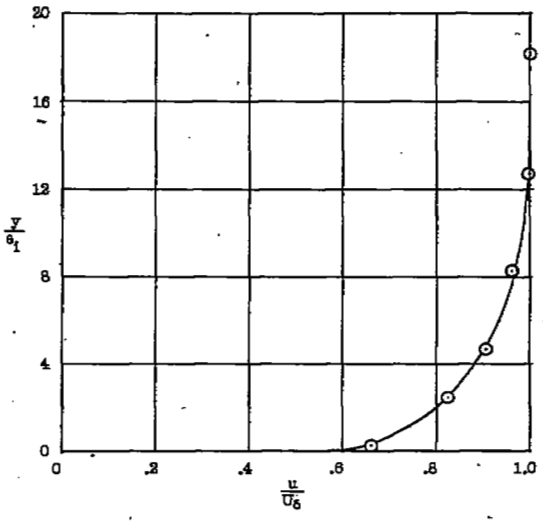

(j) Model 3; M = 2.50; θ_1 = 0.138 inch.

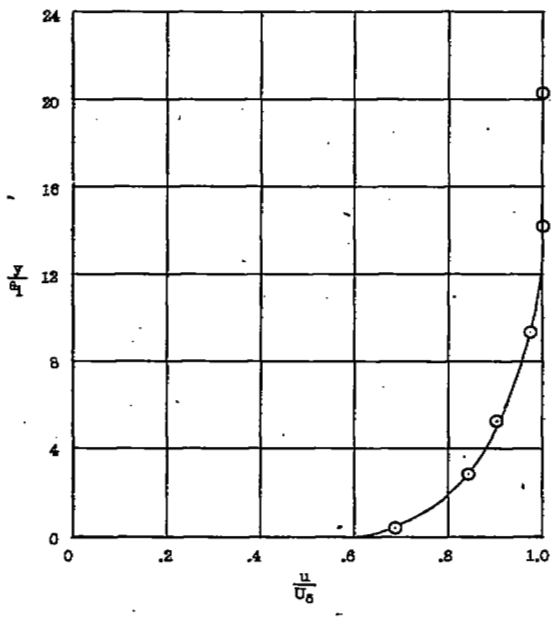

(k) Model 3; M = 3.00; θ_1 = 0.123 inch.

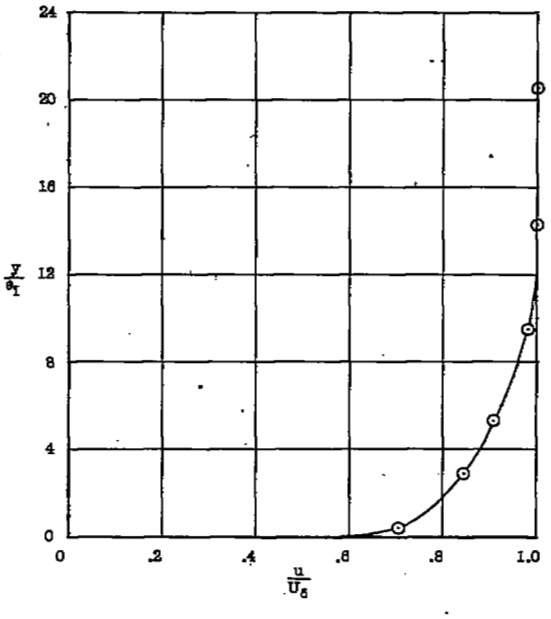

(l) Model 3, M = 3.40; θ_1 = 0.122 inch.

NACA

Figure 9.- Concluded.

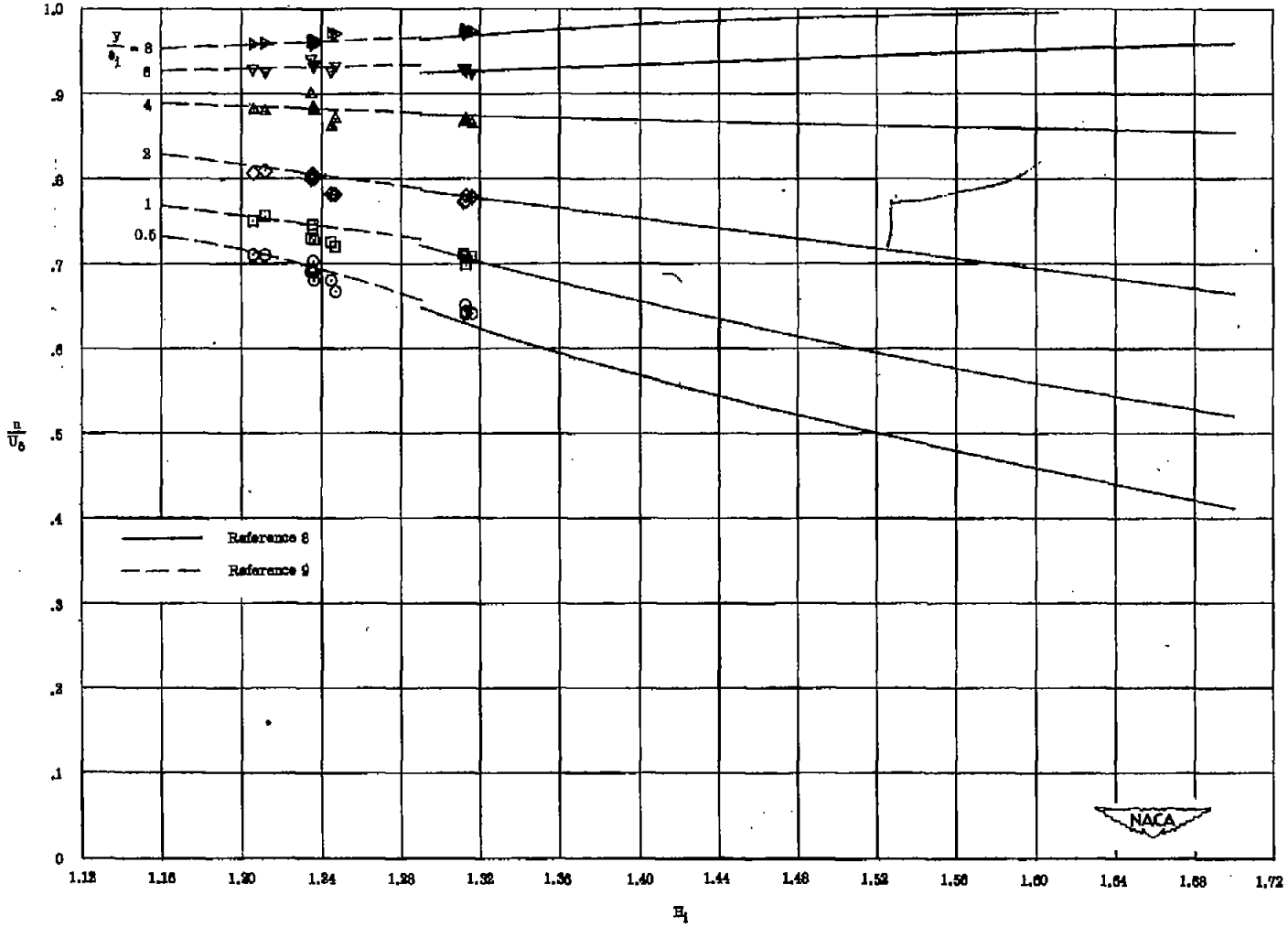

Figure 10.- Variation of $\frac{u}{U_\delta}$ with H_i for various values of $\frac{y}{\theta_i}$.

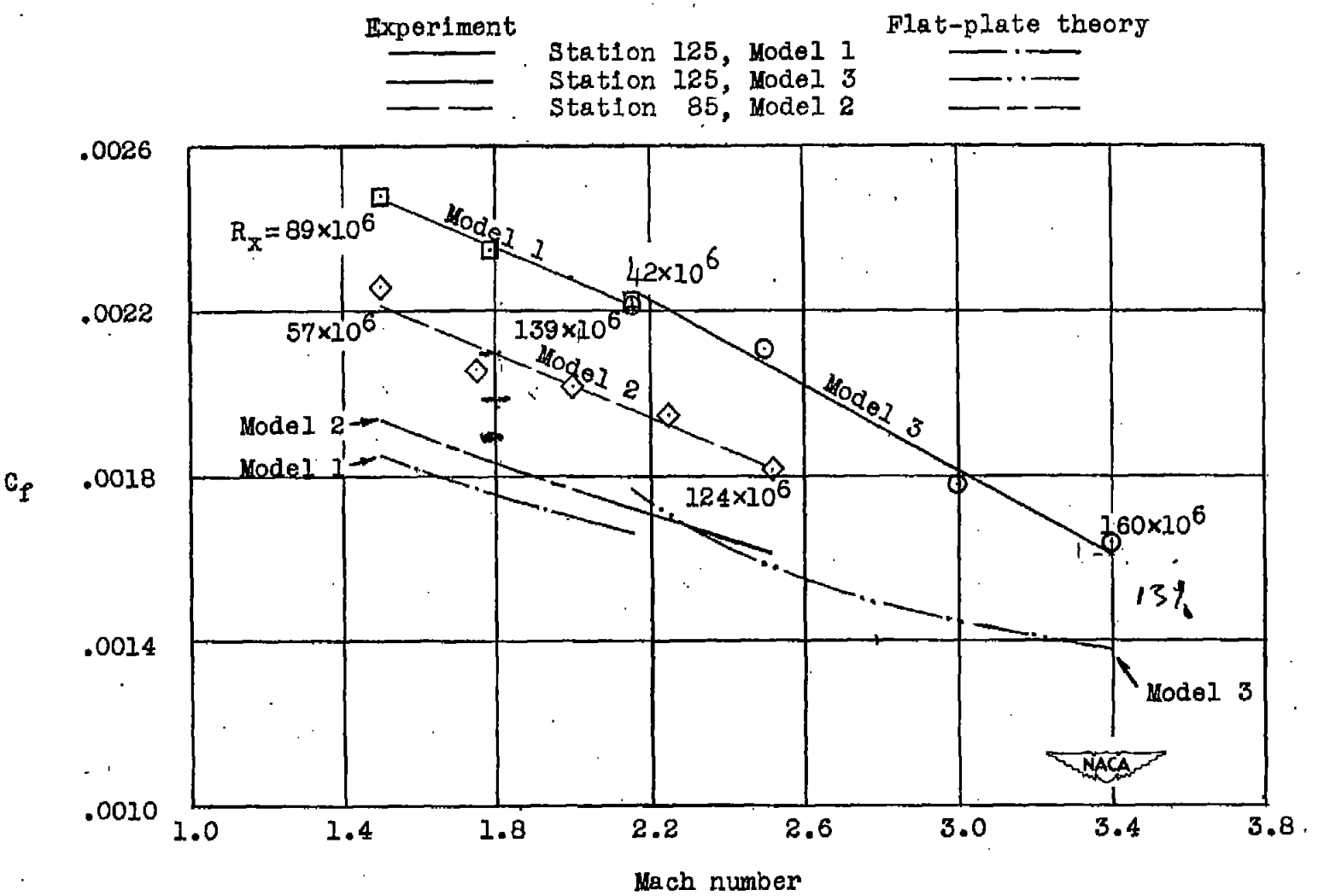

Figure 11.- Skin-friction coefficients plotted against Mach number.

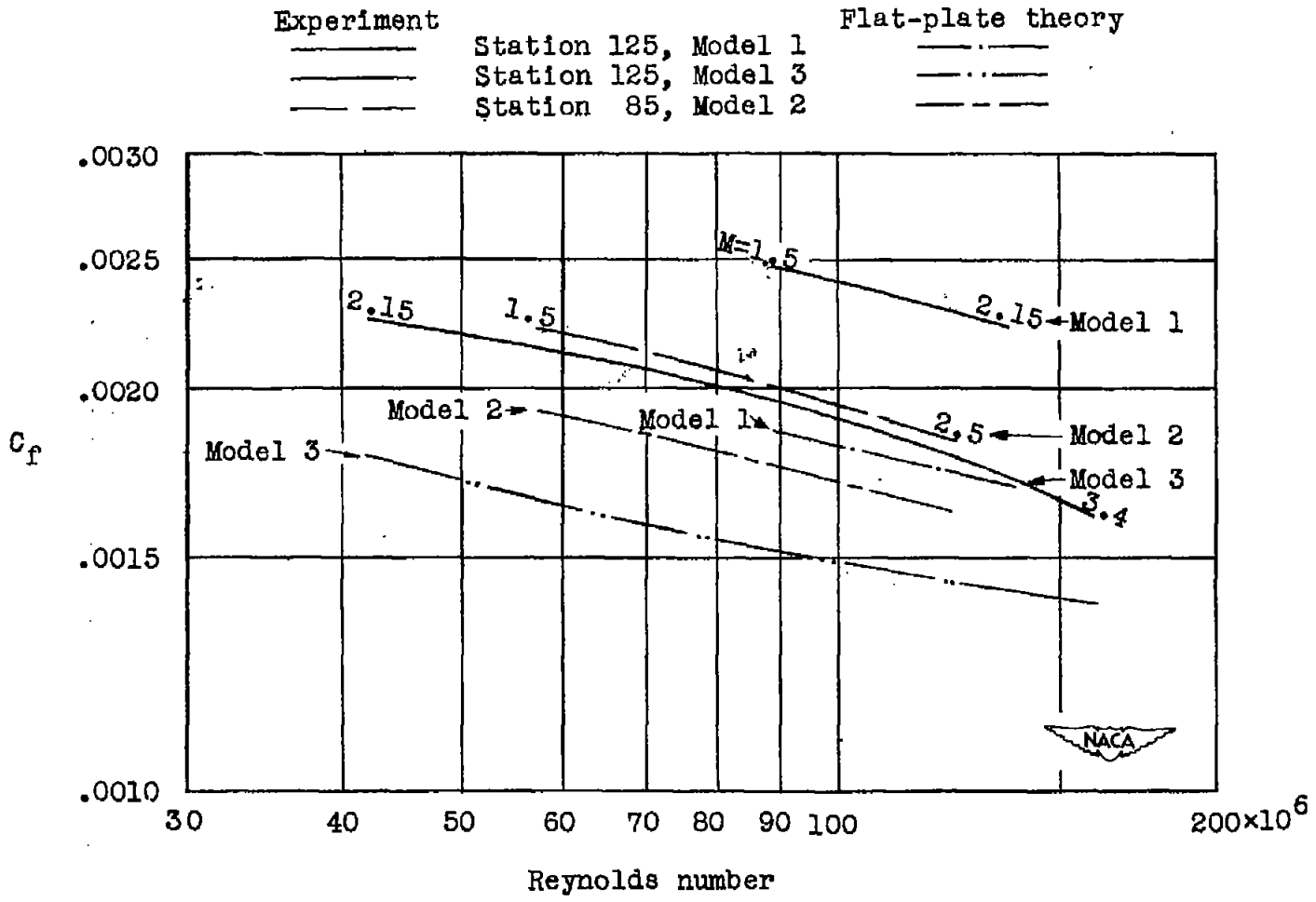

Figure 12.- Skin-friction coefficients plotted against Reynolds number. Logarithmic coordinates.

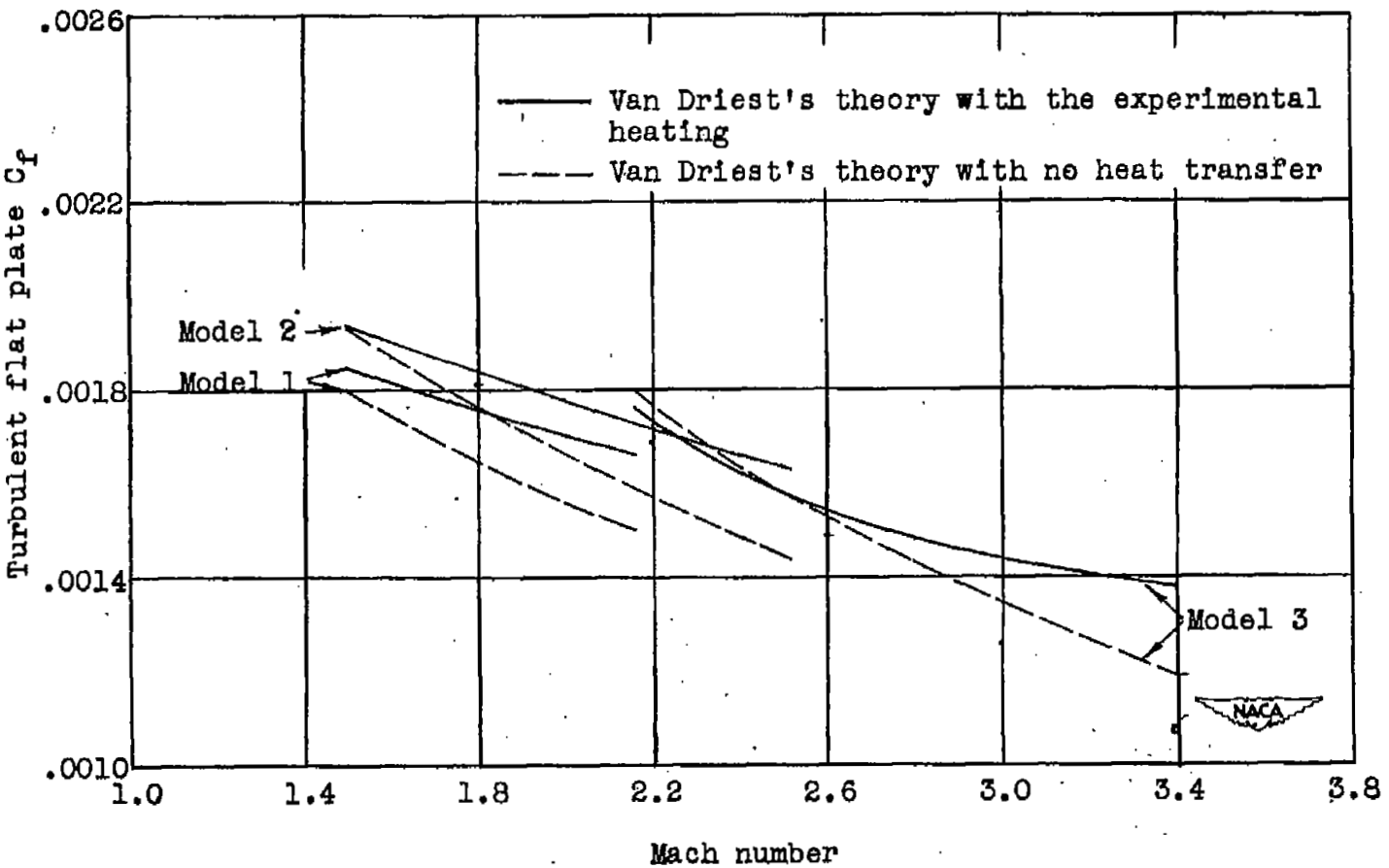

Figure 13.- Effect of the experimental heating on the theoretical flat-plate C_f.